NISTIR 5125

A Computer Model for the Diffusion and Binding of Chloride Ions in Portland Cement Paste

Dale P. Bentz
Edward J. Garboczi

Building and Fire Research Laboratory
Gaithersburg, Maryland 20899

United States Department of Commerce
Technology Administration
National Institute of Standards and Technology

NISTIR 5125

A Computer Model for the Diffusion and Binding of Chloride Ions in Portland Cement Paste

Dale P. Bentz
Edward J. Garboczi

February 1993
Building and Fire Research Laboratory
National Institute of Standards and Technology
Gaithersburg, MD 20899

U.S. Department of Commerce
Ronald H. Brown, *Secretary*

National Institute of Standards and Technology
John W. Lyons, *Director*

ABSTRACT

A two-dimensional computer model has been developed to simulate the diffusion and binding of chloride ions in cement paste. The model is based on a random walk algorithm in which chloride species randomly diffuse throughout the cement paste microstructure and interact with various phases of the paste. Reaction with unhydrated C_3A and C_4AF and adsorption by the C-S-H gel phase are the two binding processes included in the model. Input to the model is a digital image of cement paste microstructure which can be obtained from a real cement sample or from a digital-image-based microstructure model. The operation of the diffusion and binding model is demonstrated on pastes made from two cements whose differing compositions are captured by combining backscattered electron and x-ray images obtained using a scanning electron microscope. These initial images are "hydrated" using the microstructure model to produce final images to be utilized as input into the diffusion model. Chloride concentration profiles are generated for both the binding and no-binding cases for both microstructures for times of up to several hours after exposure to the chloride. Binding is seen to have a significant effect on the early-time penetration of chlorides into cement paste. Results for the two cements indicate that a higher chloride diffusion coefficient may be offset, at least initially, by a greater chloride binding capacity.

Keywords: adsorption, binding, building technology, cement, chloride ions, computer modelling, concentration profiles, diffusion, hydration, microstructure, random walk, simulation.

TABLE OF CONTENTS

ABSTRACT iii

LIST OF FIGURES vi

LIST OF TABLES vi

1. INTRODUCTION 1

2. COMPUTER MODEL DESCRIPTION 1
    2.1 GENERATION OF STARTING IMAGES 2
    2.2 CEMENT HYDRATION MODEL 4
    2.3 DIFFUSION/BINDING MODEL 6

3. REACTION AND ADSORPTION PROCESSES 9

4. RESULTS 10

5. SUMMARY 18

6. ACKNOWLEDGEMENTS 18

7. REFERENCES 18

LIST OF FIGURES

Figure 1. Images of Cements Used in Study 3

Figure 2. Reactions Used in Cement Hydration Model 5

Figure 3. Transition State Rules for Cement Hydration Model 7

Figure 4. Images of Cements after Hydration for 150 Cycles 12

Figure 5. Free Chloride Concentration Profiles after 200,000 Time Steps 13

Figure 6. Total Chloride Concentration Profiles after 200,000 Time Steps 15

Figure 7. Comparison of Chloride Concentration Profiles for Pastes of Cements 1 and 2 . 16

Figure 8. Original and Normalized Chloride Concentration Profiles for Cement 2 17

LIST OF TABLES

Table I. Composition of Cements Used in Study 2

1. INTRODUCTION

Over the past few years, in research programs sponsored by the Nuclear Regulatory Commission and the National Institute of Standards and Technology (NIST), researchers at NIST have been developing methodologies for predicting the service life of concrete structures [1]. The corrosion of reinforcing steel in concrete is a major problem limiting the useful service life of many concrete structures [2]. Chloride ions are detrimental in that they often accelerate the rate of corrosion of reinforcing steel in concrete [3] and reduce a structure's service life. When the chloride ion concentration reaches a critical level at the surface of the steel reinforcement, corrosion is initiated and may proceed rapidly. Therefore the service life of reinforced concrete structures is often effectively determined by the rate at which the chloride ion concentration builds up at the steel surface. This buildup is usually determined by the rate of penetration, from an external source, of chloride ions through the concrete cover.

In order to adequately predict the service life of a concrete structure, it is necessary to know the chloride ion diffusivity of the concrete. Experimentally, this is often difficult to assess due to sample preparation problems and the long times necessary to reach a steady-state diffusion rate [3]. Recently, however, new techniques based on impedance spectroscopy [4] or the application of an electrical field [5] have been developed. The measurement is complicated by the fact that the chloride ions interact with several components of the cement paste so that some of the chloride exists in a bound state and would thus have negligible effects on corrosion rates. These binding processes, therefore, will effectively slow down the rate of penetration of chloride ions into concrete.

In this report, a methodology based on computer modelling is developed to study the diffusion and binding of chloride ions in hydrated cement paste. Section 2 describes the microstructure model used to generate digital images of hydrated cement paste and the simulation of the diffusion and binding of chloride ions within these microstructures. Section 3 describes the diffusion/binding model parameters and provides the literature sources from which they were obtained. Early time results for two pastes made from two different cements are presented in section 4 and compared to the case where binding does not occur. Section 5 provides a summary.

2. COMPUTER MODEL DESCRIPTION

A two-dimensional (2-D) computer model has been developed for simulating the diffusion and binding of chloride ions in hydrated cement paste. A 2-D model is simpler than a three-dimensional model and requires far less computer memory, while still providing useful information on diffusion behavior. The input for the model is a two-dimensional image of cement paste microstructure. Such an image could be obtained from a scanning electron microscope (SEM) or from a microstructure model. The latter technique is utilized in this report as the digital-image-based microstructure model developed at NIST [6-7] is applied to simulating the hydration of images of actual portland cement particles.

2.1 GENERATION OF STARTING IMAGES FOR CEMENT MICROSTRUCTURE MODEL

To realistically model the microstructure development of portland cement paste, the starting images used as model input must capture the phase distribution of cement compounds within individual cement particles. Recently, experimental techniques have been developed for identifying, in an image of cement particles dispersed in a low viscosity epoxy [8], each of the five major phases of portland cement*: tricalcium silicate (C_3S), dicalcium silicate (C_2S), tricalcium aluminate (C_3A), tetracalcium aluminoferrite (C_4AF), and gypsum ($C\overline{S}H_2$). Samples are cured, polished, and viewed with the SEM. By combining information from the backscattered electron image and X-ray images for calcium, iron, aluminum, and sulfur, each solid pixel in the image may be assigned to one of the five major phases of cement. Knowing the spatial arrangement of each phase subsequently allows for a complete set of hydration reactions to be simulated as described in section 2.2.

Figure 1 shows starting images for the two cements used in this study, both at a water:cement (w/c) ratio of about 0.45. The gray scale runs from bright to dark in the order: C_3A, C_4AF, $C\overline{S}H_2$, C_3S, C_2S, and water. Phase fractions on a water-free volume basis are summarized in Table 1. Cement 1 is a standard Type I portland cement, and so is relatively high in C_3A content but low in C_4AF and C_2S. By contrast, Cement 2 is high in C_4AF and C_2S, contains only a few volume percent of C_3A, and is relatively low in C_3S. Cement 2 was ground in our laboratory and the field of view in the image in figure 1 contains phase fractions more typical of a Type II portland cement. Simulated pastes of both cements are utilized as input to the diffusion/binding simulation model.

Table I
Compositions of Cements Used In Study

Compound	Cement 1	Cement 2
C_3S	.638	.368
C_2S	.145	.398
C_3A	.132	.028
C_4AF	.045	.183
Gypsum	.040	.023

* Conventional cement chemistry notation is used throughout this document: C=CaO, S=SiO_2, A=Al_2O_3, F=Fe_2O_3, H=H_2O, and $\overline{S}$=SO_3.

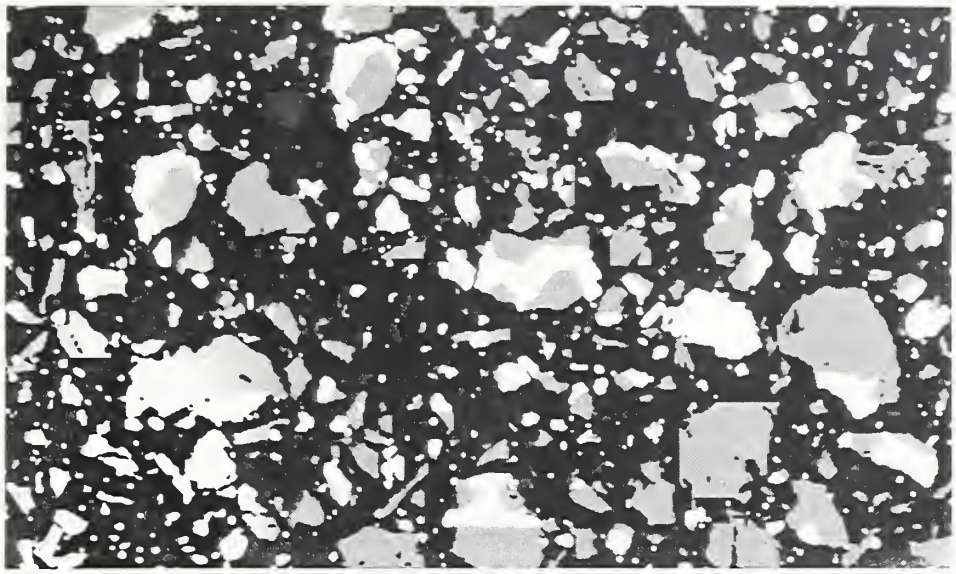

Cement 1

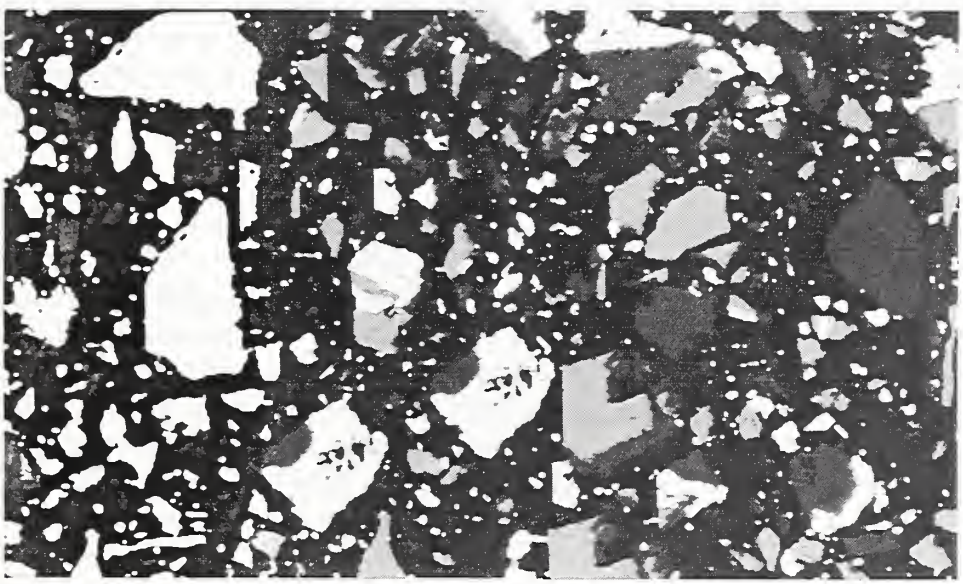

Cement 2

Figure 1. Images of Cements Used in Study.

2.2 CEMENT HYDRATION MODEL

The reactions used in the cement paste microstructure model are summarized in Figure 2. The numbers below each reaction equation indicate the volume units of each phase required to balance that particular chemical reaction. Densities and molar volumes for all phases relevant to the model were taken from the cement literature [9-10] and used to calculate these volume stoichiometries.

As seen in Figure 2, the silicate reactions are generally simpler than those for the aluminate and ferrite phases of portland cement. Tricalcium silicate, C_3S, is usually the major component of portland cement, generally present in a mass fraction of 50-70% in ASTM Type I portland cements, and is considered to be responsible for controlling many of the ultimate properties of cement-based materials including transport and strength properties. When C_3S reacts with water, a nanoporous calcium silicate hydrate (C-S-H) gel is deposited back on the surfaces of the original C_3S particles and previously deposited C-S-H, while calcium hydroxide (CH) crystals nucleate and grow in the available capillary pore space. The C-S-H gel has been shown to bind chloride ions [11] and is thus important to this study. The reactions for C_2S are similar, but less CH is formed due to the lower Ca/Si molar ratio of the initial C_2S. Additionally, in portland cement, C_2S typically reacts at a slower rate than C_3S. Due to the wide usage of pozzolanic materials such as silica fume and fly ash in concrete, the pozzolanic reaction between calcium hydroxide and reactive silica has been included in the list of reactions in Figure 2. The stoichiometry for this reaction, shown in equation (3), is based on recently published data [12] and is an approximation as it will surely vary with w/c ratio and silica fume content. In addition, C-S-H formed by the pozzolanic reaction may have different chloride binding properties than primary C-S-H [11,13].

Tricalcium aluminate, C_3A, is generally the fastest reacting phase in portland cement. In fact, gypsum is specifically added to portland cement to slow down this reaction and avoid "flash" set of the material. When gypsum is not present in the system, C_3A reacts with water to form a variety of crystalline hydration products, with hydrogarnet, C_3AH_6, being the ultimately stable hydration product [9]. Reactions are much more complex in the presence of gypsum. In this case, the C_3A will react with the gypsum to form ettringite, $C_6A\overline{S}_3H_{32}$, whose crystals are often observed to grow as needles within the cement paste. When all of the gypsum is consumed, the ettringite will decompose and react with more C_3A to form the monosulfate phase, $C_4A\overline{S}H_{12}$. The ettringite generally forms either in solution or at the surfaces of the aluminate phases in cement paste.

The reactions of the ferrite phase, C_4AF, are the least well understood of those occurring in the portland cement system. The ferrite phase generally reacts slowly (in comparison to the other phases) and contributes only to long-term properties of cements. Here, we have assumed that the reactions of the ferrite phase are similar to those of tricalcium aluminate, with extra calcium hydroxide and iron hydroxide (FH_3) produced to account for the extra calcium and iron present in the C_4AF phase [14].

Silicate Reactions

$$\underset{1}{C_3S} + \underset{1.34}{5.3H} \rightarrow \underset{1.75}{C_{1.7}SH_4} + \underset{0.61}{1.3\ CH} \quad (1)$$

$$\underset{1}{C_2S} + \underset{1.49}{4.3\ H} \rightarrow \underset{2.39}{C_{1.7}SH_4} + \underset{0.191}{.3\ CH} \quad (2)$$

$$\underset{1.34}{1.1\ CH} + \underset{1}{S} + \underset{0.67}{H} \rightarrow \underset{3.0}{C_{1.1}SH_{2.1}} \quad (3)$$

Aluminate and Ferrite Reactions

$$\underset{1}{C_3A} + \underset{1.21}{6\ H} \rightarrow \underset{1.69}{C_3AH_6} \quad (4)$$

$$\underset{0.4}{C_3A} + \underset{1}{3C\bar{S}H_2} + \underset{2.1}{26\ H} \rightarrow \underset{3.21}{C_6A\bar{S}_3H_{32}} \quad (5)$$

$$\underset{0.249}{2\ C_3A} + \underset{1}{C_6A\bar{S}_3H_{32}} + \underset{0.1}{4\ H} \rightarrow \underset{1.31}{3\ C_4A\bar{S}H_{12}} \quad (6)$$

$$\underset{0.575}{C_4AF} + \underset{1}{3C\bar{S}H_2} + \underset{2.426}{30\ H} \rightarrow \underset{3.21}{C_6A\bar{S}_3H_{32}} + \underset{0.15}{CH} + \underset{0.43}{FH_3} \quad (7)$$

$$\underset{0.358}{2\ C_4AF} + \underset{1}{C_6A\bar{S}_3H_{32}} + \underset{0.302}{12\ H} \rightarrow \underset{1.313}{3C_4A\bar{S}H_{12}} + \underset{0.093}{2\ CH} + \underset{0.266}{2\ FH_3} \quad (8)$$

$$\underset{1}{C_4AF} + \underset{1.41}{10\ H} \rightarrow \underset{1.17}{C_3AH_6} + \underset{0.26}{CH} + \underset{0.74}{FH_3} \quad (9)$$

Figure 2. Reactions Used In Cement Hydration Model

From a chloride diffusion standpoint, the unreacted C_3A and C_4AF are important since they can react with chloride ions to form Friedel's salt ($3CaO\text{-}Al_2O_3\text{-}CaCl_2\text{-}10H_2O$) [13,15]. Conversely, ettringite and other aluminate hydration products are reported not to react with the chloride ions [15]. It should be noted, however, that additional reactions could easily be included in the diffusion/binding model outlined in section 2.3.

In order to realistically simulate the microstructure development of hydrating cement, the physical processes of dissolution, diffusion, and reaction must be simulated. We model cement hydration as a three step process: 1) material first dissolves from the original cement particle surfaces, 2) then, diffuses within the available pore space, and 3) ultimately reacts with water to form hydration products. Each of these processes may be conveniently simulated using cellular automaton-type rules as described elsewhere [7]. To implement such a model, each pixel of the microstructure is processed and updated based on a set of defined rules. Reactant surface pixels may dissolve to form diffusing species. Diffusing species undergo random walk diffusion in the available pore space until reaction occurs. Both surface precipitation and nucleation and growth-type reactions can be implemented using the digital-image-based model. An example of a surface precipitation reaction would be the formation of C-S-H gel, while CH crystals form by a nucleation and growth mechanism.

The processes included in a cellular automaton-type model can be conveniently summarized in a state transition diagram such as the one shown in Figure 3 for the cement hydration model in use at NIST. Here, the arrows indicate a change of state with dissolution, nucleation, and collision (bimolecular reaction) being the possible transition processes. Diffusing species are indicated with an asterisk extension and process dependency on a variable is indicated by function notation (e.g. f[CH^*] indicates that a process depends on the diffusing CH species concentration). These rules are applied to the starting images shown in Figure 1 to create images of hydrated cement pastes to be used as input to the diffusion/binding model outlined in Section 2.3.

2.3 DIFFUSION/BINDING MODEL

Given a digital image representation of microstructure, several techniques are available for computing diffusivities. The Nernst-Einstein relation can be used to relate the relative diffusivity to a computed electrical conductivity for the microstructure [16]. Resistors can be located on the bonds connecting adjacent pixels to form a resistor network which can be reduced using numerical techniques to obtain the conductivity of the microstructure [16]. Unfortunately, this relation holds for steady-state diffusion and does not include the effects of the binding of diffusing ions by phases in the microstructure.

A second approach to computing diffusivities is to use a random walk or so-called "blind ant algorithm" [17]. Here, blind ants are released at random positions in the pore space and allowed to execute random walks. On each discrete time step, the ants attempt to move a specified distance in a random direction. The ants are blind because they do not see the solid walls distributed throughout the microstructure and therefore make no specific attempt to avoid

State Transition Diagram for Cement Hydration Model

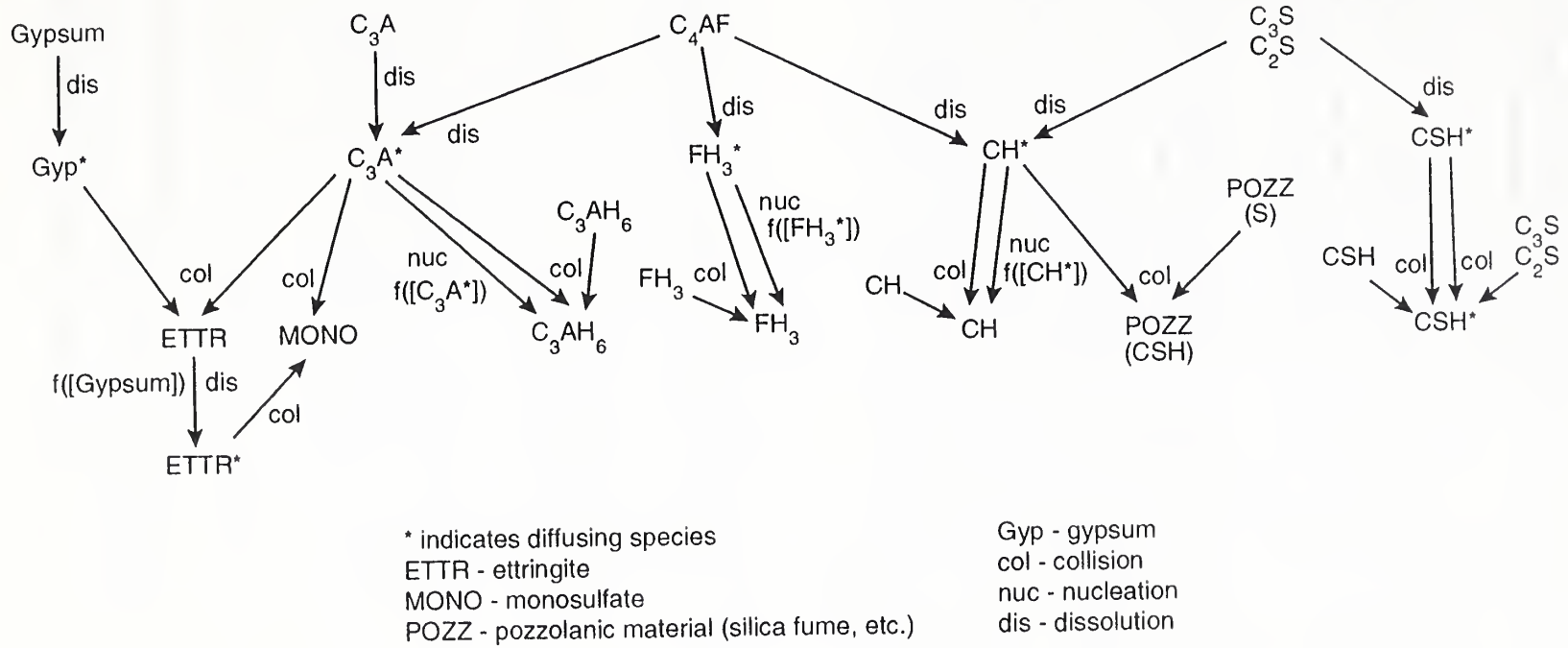

Figure 3. Transition State Rules for Cement Hydration Model.

them. If a random step would land the ant into a solid area, that step is not allowed, but time is still incremented by one unit. By computing how far an average ant travels in a given time, a diffusion coefficient for the microstructure can be calculated. This technique can be used in both continuum structures [17] and digital-image-based microstructures where the ants step from pixel to pixel [18]. This approach has the added advantage that rules can be implemented to model the reaction and adsorption of the diffusing species (blind ants) with the phases present in the microstructure, such as the C_3A and C-S-H present in a hydrated cement paste. A similar model was implemented previously for diffusion in organic coatings on steel where the diffusing species were adsorbed by pigment particles dispersed throughout the coating [19].

In the present model, the diffusion geometry chosen for the diffusion of chloride ions in cement paste was one in which a constant number concentration of diffusing species is maintained at the top surface of the microstructure. Because of the scale of the model, the diffusing species must be thought of as a collection of diffusing ions rather than as individual ions. In the model microstructures, each pixel is equivalent to a cubic micrometer (e.g., 1 μm on a side) for an image one pixel thick. Each diffusing species is considered equivalent to $1.0 * 10^{-15}$ grams of chloride ions, so that one diffusing species in a pore space pixel would represent a concentration of 1 g/l, or 0.0282 M. Each pixel may contain more than one diffusing chloride species, so the concentration of chloride ions at any point in the pore space is known to a precision of 1g/l. At each time step, each diffusing species undergoes a one-step walk to a randomly chosen neighboring pixel. The following rules are utilized for determining the outcome of this step.

1.) If the neighboring pixel is solid, then:
   a) if the neighboring pixel is C_3A or C_4AF and a reaction is favorable, then the diffusing chloride species will be consumed by the neighboring pixel to form Friedel's salt in which case it will be ineligible for further diffusion

   b) if the neighboring pixel is not C_3A or C_4AF or a reaction is not favorable, then the diffusing species remains at its present location and is eligible for further diffusion in any direction

2.) If the neighboring pixel is porous gel, then:
   a) if the neighboring pixel is C-S-H and adsorption is favorable, then the diffusing chloride species will be irreversibly adsorbed by the neighboring pixel and be ineligible for further diffusion

   b) if the neighboring pixel is not C-S-H, or is C-S-H but adsorption is not favorable, then the diffusing species is relocated to the neighboring pixel

3.) If the neighboring pixel is capillary pore space, then the diffusing species is relocated to the chosen neighboring pixel.

These rules are implemented in an iterative fashion for some specific number of steps. Output

consists of the concentration of diffusing and bound chloride species as a function of the number of time steps and depth of penetration from the exposed surface. The model can also be run in a mode where no binding occurs and these results compared to the case where chloride binding takes place.

The simulation is complicated by the fact that diffusion within the gel phases is about 400 times slower than diffusion in the capillary pores [16]. If this were simulated directly by allowing the diffusing species to move from gel pixel to gel pixel only once every 400 time steps, computer execution times would be prohibitively large. To alleviate this problem, the diffusing species are allowed to move one pixel each time step, whether the move be into a gel phase pixel or one located in the capillary pore space. This results in a certain spatial concentration profile after a given number of computational time steps. In order to then know how much real time has elapsed, it is necessary to use the true effective diffusivity, which can be computed using a direct electrical analogy as described in [16]. By fitting the exact solution for this problem to the numerical results when binding is not allowed, the diffusivity-time product Dt can be determined. Insertion of the computed true value of D then gives the real elapsed time of the simulation and thus a time scale to calibrate the computational time steps. The physical picture behind this approximation is that the cement paste is being treated as an effective continuum, with a given effective diffusivity, and with random reaction and adsorbing obstacles placed within the continuum. The exact solution for one-dimensional diffusion into an infinite half-space when the concentration at the boundary is fixed at C_o is [20]

$$C(x,t) = C_o * erfc\left(\frac{x}{2\sqrt{Dt}}\right) \qquad (10)$$

where erfc(z) is the complementary error function [20]. The simulations were not run long enough for the chloride concentration to become appreciable at the side of the sample away from the exposed surface, so that the analytical solution for an infinite half-space was applicable.

To use the model, the hydrated cement paste microstructure must be segmented into six distinct phases: capillary porosity, nonreactive solid, C_3A, C_4AF, C-S-H, and nonreactive gel phase. For the model outlined above, nonreactive solids include C_3S, C_2S, CH, C_3AH_6, gypsum, and ettringite. Nonreactive gels are FH_3 and the monosulfate phase. This segmented image is subsequently used as input for the diffusion/binding model. The chloride diffusing species can diffuse within the capillary pore space and gel phases, may react at the surfaces of C_3A and C_4AF, or may be adsorbed by the C-S-H gel. The specific rules utilized to determine the favorableness of the reaction and adsorption processes are outlined in the next section of this report.

3. REACTION AND ADSORPTION PROCESSES

The chloride ions are assumed to react only with the C_3A and C_4AF phases and to always form Friedel's salt ($3CaO\text{-}Al_2O_3\text{-}CaCl_2\text{-}10H_2O$) as the reaction product [13,15] in an irreversible

reaction. Based on the molecular weights of these compounds (270 for C_3A and 486 for C_4AF) and the stoichiometric ratio of Cl to C_3A in Friedel's salt (which is 2), one can calculate the amount of chloride ions which would be consumed by reaction with 1 g of C_3A or 1 g of C_4AF. Values of 0.263 g/ g C_3A and 0.146 g/ g C_4AF are obtained, respectively. These values can be utilized along with the densities of C_3A and C_4AF (3.03 and 3.73 g/cm^3, respectively) to determine how many Cl^- diffusing species can be consumed by one cubic micrometer (pixel) of solid material using the following equation:

$$N = integer\left(\frac{V_{pixel} * \rho * \frac{g\ Cl^-}{1\ g\ cement}}{\frac{g\ Cl^-}{1\ pixel}}\right) \quad (11)$$

where *integer* indicates the integer portion of the result, V_{pixel} is the volume of a pixel in cm^3, ρ is density of the solid material in g/cm^3, the g Cl^- /1 g of cement are given above, and $1 * 10^{-15}$ g Cl^- / pixel is assumed.

Equation 11 predicts that each pixel of C_3A may react with up to 796 diffusing species of chloride ion while each pixel of C_4AF may react with up to 544 diffusing species of chloride ion. In the model, a record is kept of how many diffusing species have reacted at each reactive solid pixel. The reactivity of the solid pixel is terminated when the above limits are reached.

The adsorption of diffusing chloride species by the C-S-H gel is based on a Langmuir adsorption isotherm, with the following equation for the bound chloride in a cement paste sample with a w/c of 0.5 [21]:

$$S_{Cl^-} = \frac{\alpha * C_{Cl^-}}{1 + \beta * C_{Cl^-}} \quad (12)$$

where S is expressed in mmole/g cement and C is expressed in mole/liter. Values of $\alpha = 1.67$ and $\beta = 4.08$ were determined to best fit the bound chloride vs. free chloride data [21]. It should be noted that at very high chloride concentrations, these values would correspond to 1.45 g Cl^-/ 100 g C-S-H. This value is in general agreement with the results of Beaudoin et al [11] who measured Cl^- binding of C-S-H as a function of Ca/Si molar ratio and found alcohol-insoluble Cl^- to be equal to 0.01+0.89*(Ca/Si) in percent by mass of cement. For a Ca/Si molar ratio of 1.7, this corresponds to 1.52 g Cl^- /100 g C-S-H.

4. RESULTS AND DISCUSSION

Both of the 500 x 500 pixel (500 x 500 μm, w/c=0.45) images shown in Figure 1 were "hydrated" for 150 cycles using the 2-D microstructure model. These are small samples, and can only show a maximum penetration of 0.5 mm. Real experiments are usually done down to a depth of about five centimeters [15,21], the usual cover thickness of concrete on top of

reinforcing steel. For Cement 1, high in C_3A, a degree of hydration of 0.785 was attained, resulting in a capillary porosity of 18.0%. The total area fraction of gel plus capillary pore space for Cement 1 was 0.663. For the coarser Cement 2, high in C_4AF, a degree of hydration of 0.64 was attained, with a capillary porosity of 23.2% and a total area fraction of gel plus capillary pore space of 0.70. The gel area fraction alone was almost identical for the two cement pastes. The final microstructures obtained after these amounts of hydration are shown in Figure 4. The effective two-dimensional relative diffusivity was computed to be 0.00074 and 0.0014 for Cements 1 and 2, respectively. The relative diffusivity is defined as D/D_o, where D is the bulk measured value of diffusivity and D_o is the value for chloride ions diffusing, at a given temperature, in free water. The value of D_o used in this report is $1.5 * 10^{-9}$ m^2/s [22, at 25°C]. These values of D/D_o indicate that chloride ions, for instance, would have a diffusivity in these microstructures of about one thousandth of their value in free water. The lower value observed for Cement 1 is consistent with its higher degree of hydration and lower capillary porosity. These results indicate that when comparing the spatial chloride concentration profiles obtained for the two cement pastes, the real time per computational step for Cement 1 will be about twice as long as that for Cement 2.

Random walk simulations were conducted for up to 200,000 time steps for both microstructures, for both the binding and no-binding (via reaction and adsorption) cases while maintaining a constant surface concentration of six diffusing species per pixel, equivalent to a 0.17 M solution of chloride ions ponded on the surface. Concentration profiles were computed every 5000 time steps, but only a subset of the results are presented here to demonstrate the effects of reaction and microstructure on concentration profiles. The total binding capacity of Cement 1 was 1.64 grams of chloride per liter of paste, while for Cement 2 the total binding capacity was 13.2 g/l, a factor of eight larger. The total binding capacity is computed assuming all the C_3A and C_4AF present reacts completely with chloride ions. The total binding capacity does not include adsorption due to gel phases, but since both pastes contain almost identical amounts of gel phases, they will also have about the same potential for adsorption of chloride ions in these phases.

Figures 5(a) and 5(b) show the concentration profiles for the two cements, averaged over the cross-section of the sample, for the binding and no-binding cases after 200,000 time steps. By approximately fitting the numerical data for both cement pastes to the exact solution for the case of no binding given in equation 10, we find that the time scale for Cement 1 is about 0.05 seconds/time step, while that for Cement 2 is about 0.029 seconds/time step. The time corresponding to 200,000 time steps would then be about 3 hours for Cement 1 and 1.5 hours for Cement 2, so these results apply only to the early time behavior of chloride diffusion and binding in cement paste. As would be expected, the binding greatly slows down the progression of the diffusion front. For example, in Fig. 5b for Cement 2, a concentration level of at least 1 g/l is present up to a distance of 64 μm for the binding case, but persists until 203 μm for the no-binding case, a factor of more than three times as far. Similar results are observed for Cement 1 but here the equivalent distance factor is only about two, due to the smaller binding capacity of this cement paste.

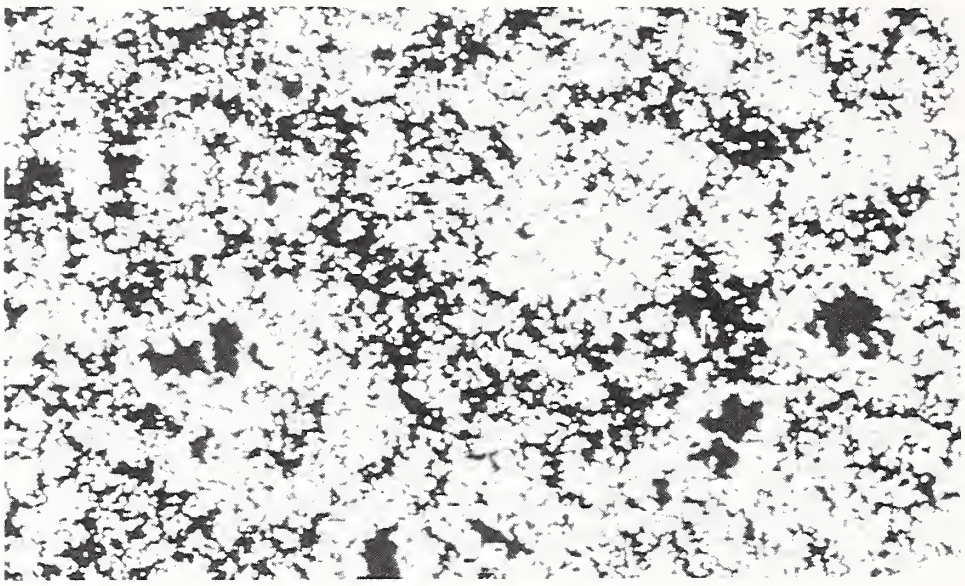

Cement 1

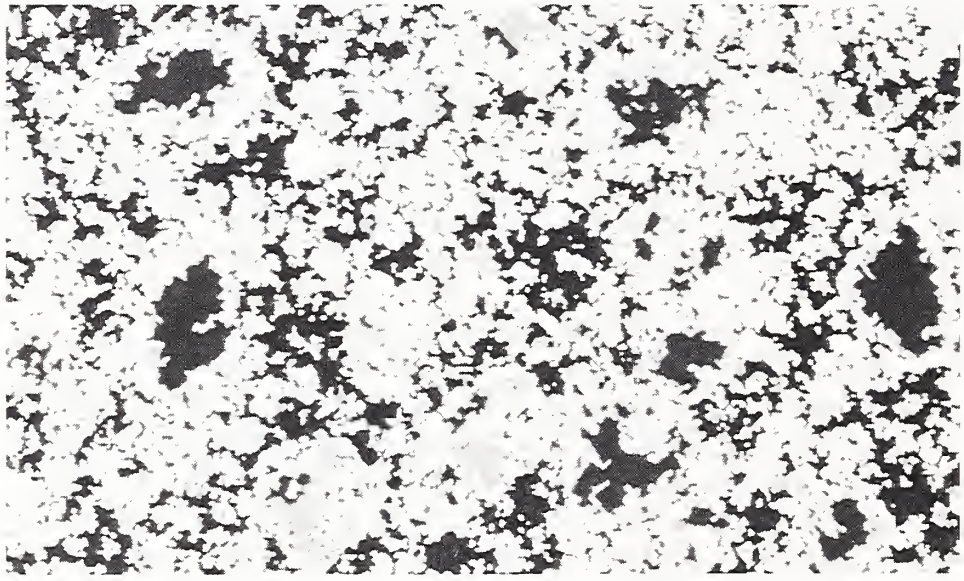

Cement 2

Figure 4. Images of Cements after Hydration for 150 Cycles.

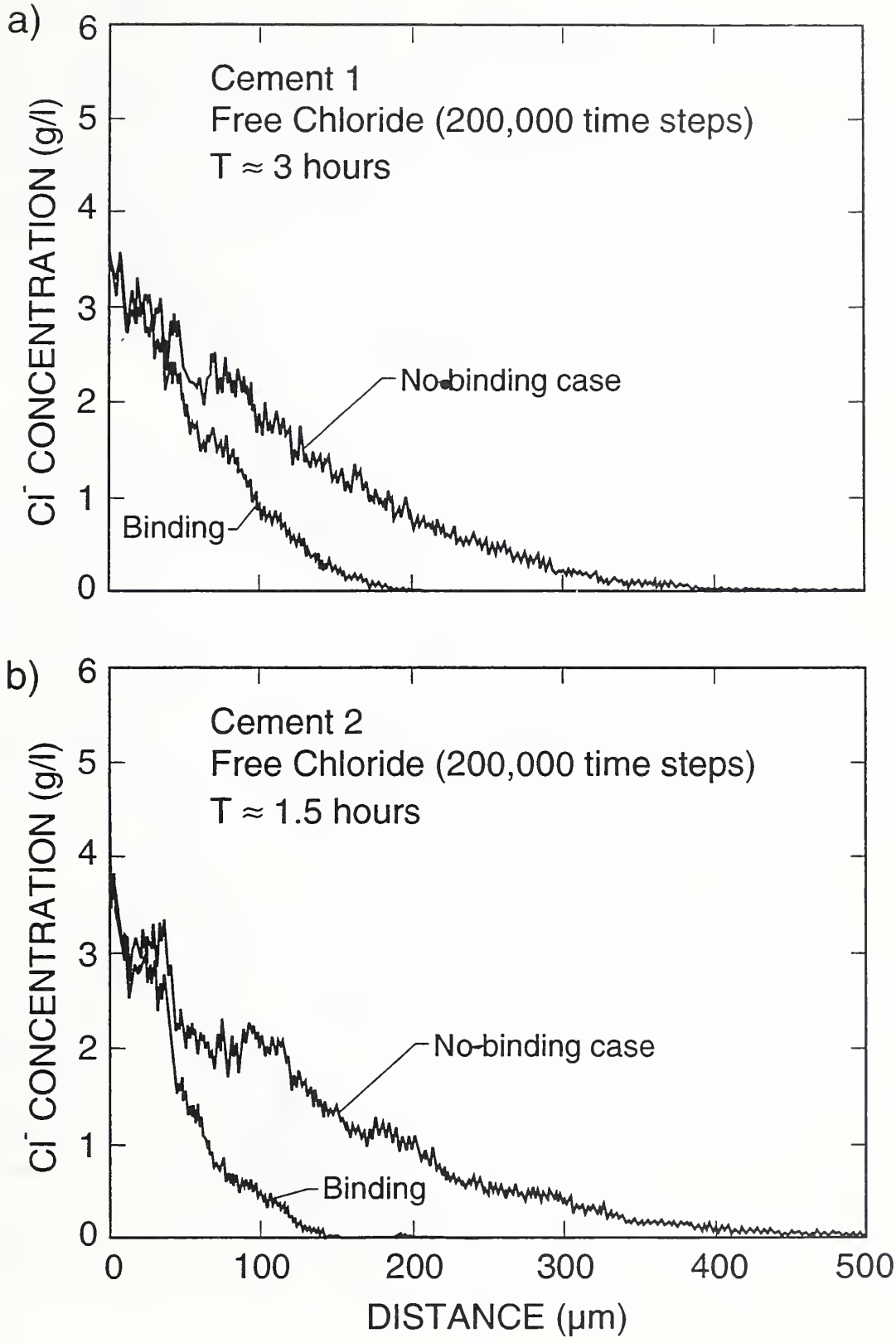

Figure 5. Free Chloride Concentration Profiles.

The equivalent plots for total chlorides are shown in Figure 6. Here, we see that the samples where reactions and adsorption are present contain a larger concentration of chlorides near the surface of the sample than the samples where no binding occurs. In fact, the concentration near the surface even exceeds the constant surface concentration of 0.17 M (6 g/l) maintained at the top surface throughout the simulation. This phenomena has been observed experimentally, where sometimes in sectioning concrete and determining chloride content, the top section will contain a greater concentration of total chlorides than the solution to which it was exposed [23]. The plots for total chloride appear much noisier than those for free chlorides. This phenomenon is due to the fact that the remaining unhydrated C_3A and C_4AF are distributed nonuniformly throughout the 2-D microstructure so that the level of reaction at a given depth is quite variable, which adds another source of randomness to the intrinsic randomness of the diffusion process itself. This noise would be smoothed out if a larger sample were utilized as the phase distributions should then be more uniform.

Since Cement 2 does have a greater chloride binding capacity than Cement 1, mainly because it contains more unhydrated C_4AF to react with the chloride ions, it is interesting to compare the chloride penetration profiles of the two cement pastes at equivalent times. As stated earlier, the relative diffusivity of Cement 2 is about twice that of Cement 1 so we will compare concentration profiles obtained after 100,000 time steps for Cement 1 and after 200,000 time steps for Cement 2. These results are plotted in Figure 7 for the a) no-binding and b) binding cases. First, for the no-binding case, we observe that chlorides have progressed farther into Cement 2. Interestingly, however, for the binding case, the two chloride concentration profiles are almost identical. Once again, this is due to the greater binding capacity of Cement 2. Even though it is less resistant to diffusive transport, it binds a greater number of chlorides so that the free chlorides are similar to those observed for Cement 1. This simple example illustrates that both the steady-state diffusion coefficient and the binding capacity of a cement are important in determining the actual penetration of chlorides into a cement-based material, particularly during early exposure times before steady-state transport is achieved.

In general, the plots for free chlorides look quite similar to those that would be expected for Fickian diffusion in a homogeneous media. However, some sharp drops in the concentration profiles can be observed. These dropoffs have been correlated with regions in the microstructure where there is a sharp decrease in the phases available for transport (gel and capillary porosity) as a function of depth. To reduce this effect, concentrations can be normalized at each depth by dividing by the volume of phases available for local transport. Normalized and original concentration profiles are shown in Figure 8 for Cement 2 in the case where no binding of chlorides is present. A large portion of the variability (from a smooth curve) in the original concentration profile is eliminated when the curve is normalized by the phase volume locally available for diffusion. Of course in a real experiment, measurements cannot be made every micrometer, but perhaps every millimeter. Integrating over the micrometer-scale noise in the numerical data would also tend to greatly smooth the concentration profiles. Similar variability in concentration data might be observed in concrete due to local variability in aggregate content as a function of depth.

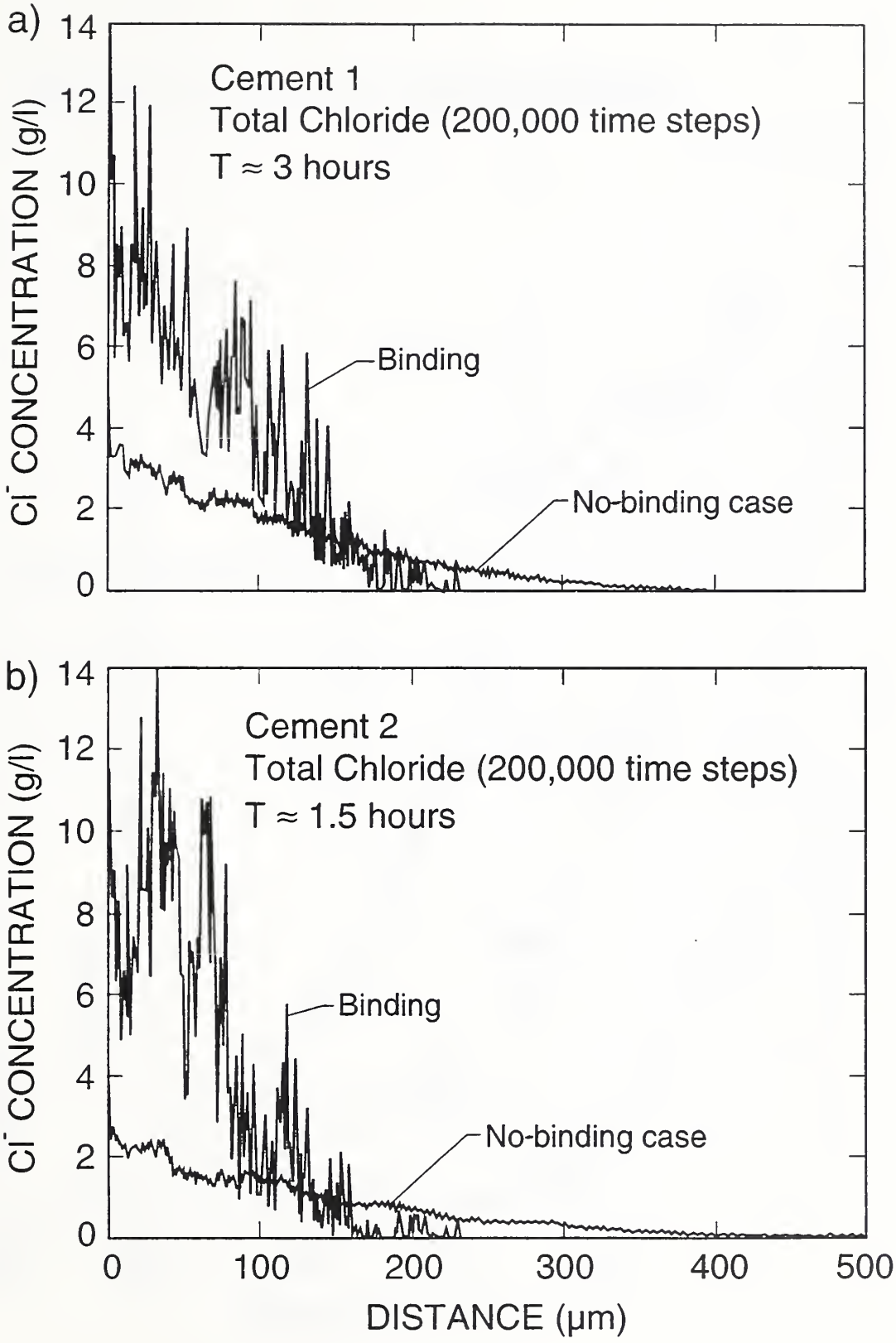

Figure 6. Total Chloride Concentration Profiles.

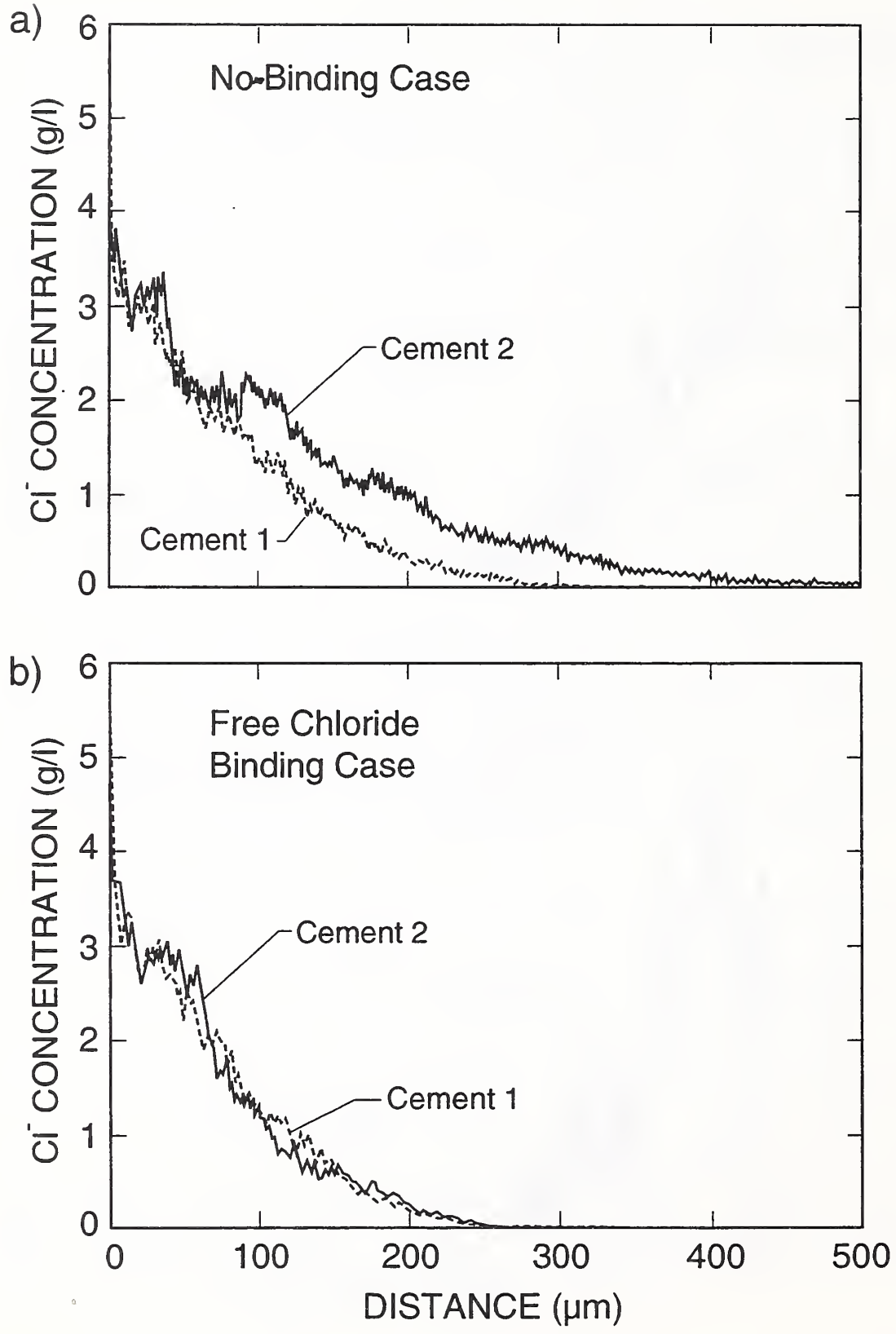

Figure 7. Comparsion of Chloride Concentration Profiles for Pastes of Cements 1 and 2.

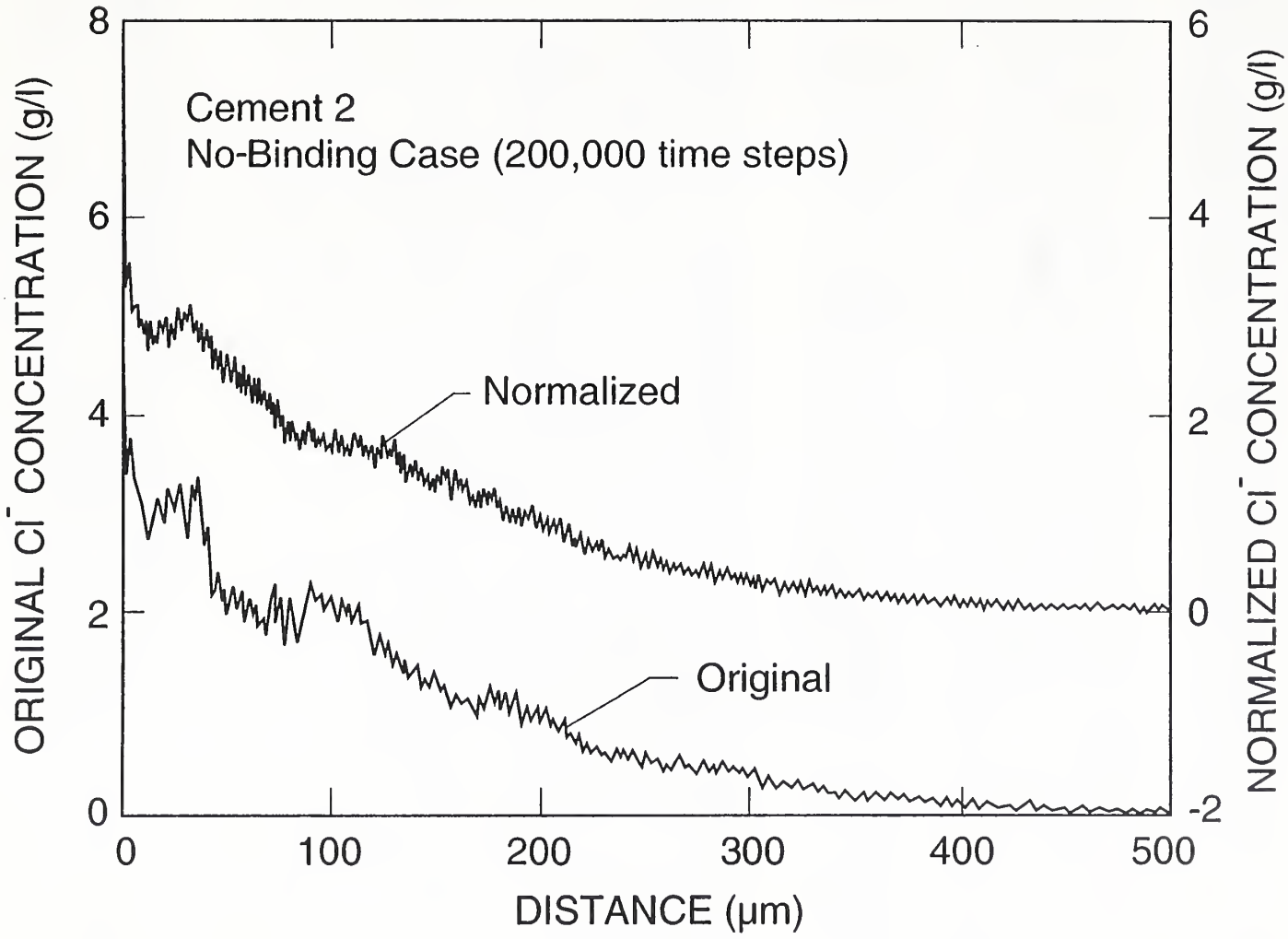

Figure 8. Original and Normalized Chloride Concentration Profiles for Cement 2.

5. SUMMARY

A two-dimensional digital-image-based model has been developed for simulating the diffusion and binding of chloride ions in hydrated cement paste. The model contains the simplifying assumptions of two-dimensionality and the use of an effective relative diffusivity to scale the results.

The results of this study indicate that:

1) Binding (reaction and adsorption) processes can substantially slow the penetration of chloride ions into cement, especially at early times. Ultimately, of course, the maximum binding capacity will be achieved locally.

2) Both the diffusivity and the binding capacity of a material are important in limiting chloride ion ingress. As illustrated by the two cements studied, a cement with a higher diffusivity such as Cement 2 may resist chloride ion penetration as well as a cement with a lower diffusivity if it is able to bind more chloride ions.

The model described could be extended to three dimensions and longer diffusion times, given adequate computer memory and time. For example, a three-dimensional simulation where the sample considered is 200 μm x 200 μm x 5 mm would require a unit cell size of 200 x 200 x 5000 pixels, with at least 1.6 gigabytes of computer memory. Another technical obstacle to three-dimensional simulations has been in creating three-dimensional cement particles which accurately represent the intra-particle clinker phase distributions of interest. Work is ongoing to develop techniques to translate the two-dimensional images shown in Figure 1 into their three-dimensional counterparts. Diffusion is only one of the transport mechanisms vital to the service life of concrete. Capillary flow and flow under pressure may also contribute to the ingress of chloride ions into a microstructure, particularly if the specimen is exposed to wetting and drying cycles [23]. Research is underway at NIST to study dispersion of a species in a porous media due to convection and diffusion at various Peclet numbers [24] which should ultimately lead to a greater understanding of how microstructure affects the transport of deleterious species into a cement-based material.

6. ACKNOWLEDGEMENTS

The authors would like to thank Paul Stutzman of the Building Materials Division for assistance in obtaining the original cement particle images of the two cements used in this study and Dr. James Clifton for several useful conversations.

7. REFERENCES

1) Clifton, J.R., "Predicting the Remaining Service Life of Concrete", NISTIR 4712, U.S. Department of Commerce, November, 1991.

2) Clifton, J.R., and Knab, L.I., "Service Life of Concrete", NISTIR 89-4086, U.S. Department of Commerce, November 1989.

3) Clifton, J.R., Knab, L.I., Garboczi, E.J., and Xiong, L.X., "Chloride Ion Diffusion in Low Water-To-Solid Cement Pastes", NISTIR 4549, U.S. Department of Commerce, April 1991.

4) Christensen, B.J., Mason, T.O., Jennings, H.M., Bentz, D.P., and Garboczi, E.J., "Experimental and Computer Simulation Results for the Electrical Conductivity of Portland Cement Paste", in Advanced Cementitious Systems: Mechanisms and Properties, MRS Syp. Proc., 245, pp. 259-264, 1992.

5) Luping, T., and Nilsson, L., "Rapid Determination of the Chloride Diffusivity in Concrete by Applying an Electrical Field", ACI Materials Journal, 89 (1), pp. 49-53, 1992.

6) Bentz, D.P. and Garboczi, E.J., "A Digitized Simulation Model for Microstructural Development", in Advances in Cementitious Materials, Ceramic Transactions, 16, pp. 211-226, 1991.

7) Bentz, D.P., Coveney, P.V., Kleyn, M.E., Garboczi, E.J., and Stutzman, P.E., "Cellular Automaton Simulations of Cement Hydration and Microstructure Development", submitted to Modelling and Simulation in Materials Science and Engineering.

8) Bentz, D.P., and Stutzman, P.E., "Combination of SEM Backscattered Electron and X-ray Map Images to Identify Phases in Portland Cement", to be presented at ASTM Symposium on the Petrography of Cementitious Materials, Atlanta, GA, June 1993.

9) Young, J.F., and Hansen, W., in Microstructural Development During Hydration of Cement, edited by L.J. Struble and P.W. Brown (Materials Research Society, Pittsburgh, PA, 1987).

10) Mindess, S., and Young, J.F., Concrete, (Prentice-Hall, Englewood Cliffs, NJ, 1981).

11) Beaudoin, J.J., Ramachandran, V.S., and Feldman, R.F., "Interaction of Chloride and C-S-H", Cement and Concrete Research, 20, pp. 875-883, 1990.

12) Lu, P., Sun, G.K., and Young, J.F., "Phase Composition of Hydrated DSP Cement Pastes", Journal of the American Ceramic Society, in press.

13) Page, C.L., and Vennesland, O., "Pore Solution Composition and Chloride Binding Capacity of Silica Fume Cement Pastes", Materials and Structures, 16, pp. 19-25, 1983.

14) Brown, P.W., "Early Hydration of Tetracalcium Aluminoferrite in Gypsum and Lime-Gypsum Solutions", Journal of the American Ceramic Society, 70 (7), pp. 493-496, 1987.

15) Midgley, H.G., and Illston, J.M., "The Penetration of Chlorides into Hardened Cement Pastes", Cement and Concrete Research, 14, pp. 546-558, 1984.

16) Garboczi, E.J., and Bentz, D.P., "Computer Simulation of the Diffusivity of Cement-Based Materials", Journal of Materials Science, 27, pp. 2083-2092, 1992.

17) Schwartz, L.M., and Banavar, J.R., Phys. Rev., B39, 11965, 1989.

18) Garboczi, E.J., and Bentz, D.P., "Analytical and Numerical Models of Transport in Porous Cementitious Materials", Materials Research Society Symposium Proceedings, Pittsburgh, PA, 176, pp. 675-81, 1990.

19) Bentz, D.P. and Nguyen, T., "Simulation of Diffusion in Pigmented Coatings on Metals Using Monte-Carlo Methods", Journal of Coatings Technology, 62 (783), pp. 57-63, 1990.

20) Crank, J., The Mathematics of Diffusion, pp. 20-21, (Oxford University Press, England, 1975).

21) Sergi, G., Yu, S.W., and Page, C.L., "Diffusion of Chloride and Hydroxyl Ions in Cementitious Materials Exposed to a Saline Environment", Magazine of Concrete Research, 44, pp. 63-69, 1992.

22) Handbook of Chemistry and Physics, ed. Robert C. Weast, 57th edition (CRC Press, Cleveland, 1976), p. F-62.

23) Page, C.L., Lambert, P., and Vassie, P.R.W., "Investigations of Reinforcement Corrosion. 1. The Pore Electrolyte Phase in Chloride-Contaminated Concrete", Materials and Structures, 24, pp. 243-252, 1991.

24) Martys, N.S., unpublished results.